Int. J. Electrochem. Sci., 15 **(2020)** 94 – 108, doi: 10.20964/2020.01.24

International Journal of
ELECTROCHEMICAL
SCIENCE
www.electrochemsci.org

Modelling of Geometric Features of Micro-Channel Made using Abrasive Assisted Electrochemical Jet Machining

Changshui Gao[£], Zhuang Liu[£,], Yi Qiu, Kai Zhao*

College of Mechanical and Electrical Engineering, Nanjing University of Aeronautics and Astronautics, 29 Yudao Street, Nanjing 210016, China;
[£]These authors contributed equally to this work and should be considered co-first authors
[*]E-mail: liuzhuang@nuaa.edu.cn

Received: 6 August 2019 / *Accepted:* 6 October 2019 / *Published:* 30 November 2019

Geometric features of micro-channel can significantly affect heat transfer rate or fluid mixing rate in applications where the micro-channels are functioning. Abrasive assisted electrochemical jet machining (AECJM) can machine complex micro-channels at metals with low-cost, high efficiency and good surface quality. This study presented a method for predicting channel width and channel depth machined using AECJM process. Two different models, namely quadratic polynomial model and dimensional analysis model, for predicting width and depth of micro-channel due to AECJM were developed and investigated. The result shows that the dimensional analysis model has more stable predictability than quadratic polynomial model. Jet diameter is the dominant factor affecting the channel width, while working voltage and machining time are main factors influencing the channel depth. The inter-relationship between channel width and channel depth can be expressed using presented predictive models. Afterwards, micro-channel with desired width and depth can be achieved through the inter-relationship and present models.

Keywords: micro-channel; geometric features; abrasive assisted electrochemical jet machining; electrochemical jet machining; abrasive water jet machining

1. INTRODUCTION

The structure of micro-channels has been increasingly used in industries for heat exchanging, fluids flow and fluids mixing. For example, micro-channel heat sink is a type of small heat transfer device in which micro-channels are patterned to dissipate heat efficiently so as to keep the electronic components working properly [1-2]. It also can be used in areas of biochemical analysis, medical diagnostics, drug delivery and micro-reactors where rapid mixing of species is needed [3]. Geometric features of micro-channel (e.g. channel shape, width and depth) will impact heat transfer or mixing rate significantly. For instance, Zhang et al [2] investigated the effect of three micro-channel shapes on

cooling performance and found that it can be improved by optimization of the channel depth and width. Walunj et al [4] reported a study of pool boiling heat transfer and revealed that modification of channel geometries resulted in a maximum of 169% enhancement of the heat transfer rate. Therefore, how to control geometric features has become a research focus in manufacturing of micro-channel.

Technologies able to fabricate micro-channels at metals include micro-milling [5], laser machining [6], electro-discharge machining [7], electrochemical machining[8], biomachining [9] and jet machining etc [10-11]. Among these processes, abrasive assisted electrochemical jet machining (AECJM) is a hybrid process capable of manufacturing micro-channels at a variety of metals [12-14] with advantages of low-cost and high efficiency. As illustrated in Fig.1, the AECJM process combines electrochemical jet machining (ECJM) and abrasive water jet machining concurrently. The material removal of AECJM involves: (I) the mass loss due to anodic dissolution, (II) the mass loss due to erosion, and (III) the mass loss due to removal of passivation layer.

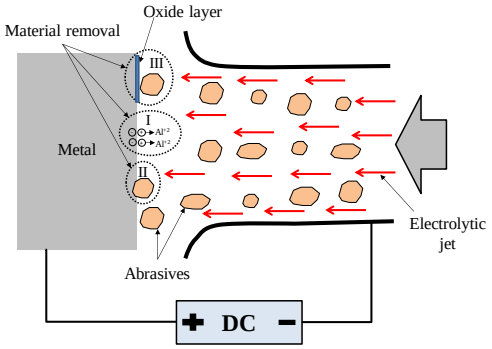

Figure 1. Schematic of material removal of AECJM

This complicated mechanism of material removal causes great difficulty to develop theoretical models to identify each proportion of the three types of removal. Consequently, describing the evolution of machining surface can't be implemented as well. Up to date, most researches of AECJM have focused on mechanism of material removal and effect of processing factors on machining result. For example, Liu et al. [12] investigated synergistic effect of erosion and corrosion in AECJM of cobalt-based alloy. Zhang et al. [13] discussed effects of electrolytic concentration, working voltage and jet pressure on material removal rate in AECJM of SUS304. Fan et al. [14] and Liu et al. [15] studied AECJM of SKD11 mold steel and tungsten carbide respectively, and found that the abrasives can break oxide layer generated on the machining surface and subsequently increase the material removal rate of AECJM.

Recently, Liu et al. [16] proposed an empirical model for predicting width and depth of micro-channel due to AECJM process. The model was expressed as a pair of nonlinear equations in which the output is a product of six process factors with exponentials. The drawback of this model is that the dimensions of the variables are inhomogeneous so that the importance of each process factor on result can't be well understood. Furthermore, it lacked expression of relationship between channel width and channel depth in applying the model. Thus, this study aims to overcome the shortcomings of above-

mentioned work and improve the measure of controlling geometric features in AECJM of micro-channel.

Dimensional analysis is a commonly used modelling approach dealing with prediction of practical problems. It is based on the hypothesis that the physical process can be expressed by means of a dimensionally homogeneous equation in terms of specific variables. Recently, Chevalier et al. [17] developed a current density distribution model using this approach along the channel of a polymer electrolyte membrane fuel cell. Ferro et al. [18] applied this modelling measure to build up a flow resistance equation theoretically. In the field of machining technology, dimensional analysis has also been paid attention to describe the relationship between machining result and process factors. For example, Kumar et al. [19] developed a model for predicting material removal rate in ultrasonic machining of titanium using dimensional analysis and orthogonal experiment. Patil et al. [20] used dimensional analysis to construct a semi-empirical model for predicting material removal rate in wire EDM process in terms of thermo-physical properties of work piece and machining parameters.

Quadratic polynomial model, normally expressed as a sum of terms of main factors, two-factor interactions and higher-order factors [21], is another important tool for empirically mapping the relationship between response of a process and its input variables [20]. Many research works have applied this approach to predict machining result in terms of process factors. For instance, Sankar et al. [22] developed a model to forecast material removal rate in processing composite by abrasive assisted electrochemical machining. Zhao et al. [23] experimentally derived a set of quadratic models for predicting surface roughness in ultrasonic vibration cutting of Inconel alloy. Kumaran et al. [24] also employed this modelling method to predict surface roughness in abrasive water jet machining of carbon fiber-reinforced plastics composites.

The objective of this study is to compare the performance of two different models developed using above reviewed two modelling approaches for predicting channel width and depth due to AECJM. The relationship between channel width and depth also has been investigated for design of target channel. Finally, this paper presented complex micro-channels with desired width and depth machined using the proposed model.

2. EXPERIMENTAL CONDITIONS

Fig.2 illustrates the schematic of AECJM experimental apparatus used in the present work. As shown in the figure, a fluidic jet, which is mixed with electrolyte and Al_2O_3 abrasives, is pressurized and propelled to flow through a micro-sized orifice, and impinges to the surface of a metallic specimen where the material will be removed by anodic dissolution and particles erosion concurrently. A current supply, of which negative and positive poles are connected with metallic orifice and specimen respectively, is used to provide necessary potential for the electrochemical reaction in the process. A XY stage mounts the specimen and drives it along a pre-designed trajectory of the machining channel during the process.

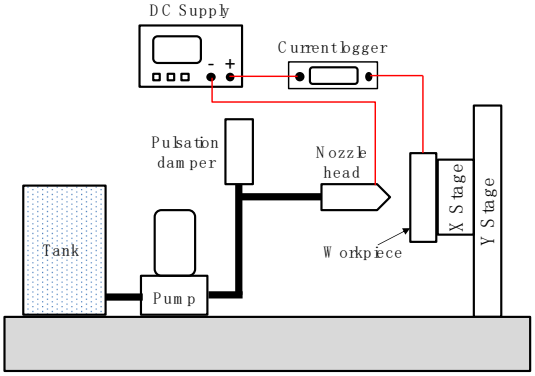

Figure 2. Schematic of AECJM process.

Table 1 shows the experimental conditions in this study. The specimen was prepared using material of stainless steel 316. The fluidic jet is mixed with tap water, 15wt% $NaNO_3$ and Al_2O_3 abrasives with 1500 mesh size. This jet is formed as a size of 150 μm in diameter using an orifice with the same size. The jet is adjusted to impact the specimen vertically. The standoff distance between orifice and target keeps as 2 mm for the consideration of machining stability. Other process conditions, such as working voltage, concentration of abrasives, jet pressure, jet scan speed and number of jet scan passes, would be managed in different levels in the machining.

Table 1. Summary of experimental parameters used in this study.

Jet diameter and impact angle	150 μm, 90 º
Jet pressure	Variation 3 to 4 MPa
Standoff distance	2 mm
Abrasive type and concentration	1500 mesh sized Al_2O_3, variation 0.3 to 0.9 wt%
Electrolyte composition	15 wt% $NaNO_3$
Working voltage	DC, variation 100 to 160 V
Jet scan speed	Variation 0.04 to 0.08 mm/s
Number of jet scan passage	Variation 4 to 10
Target material	Stainless steel 316

Fig. 3 demonstrates two key geometric features, i.e. channel width (*W*) and channel depth (*H*), which are interested and needed to be controlled for possible applications. Obviously, almost all the parameters in Table 1 can affect channel width and depth to some extent, however, the significance of each parameter on that is different. Some of the parameters are inconvenient to be regulated during the process; others, on the other hand, are easy to control during the machining. Therefore, this study chose five parameters, i.e. working voltage (*U*), concentration of abrasives (*A*), jet pressure (*P*), jet scan speed (*V*) and number of jet scan passage (*N*), as variations to predict the width (*W)* and depth (*H)* in AECJM of micro-channels.

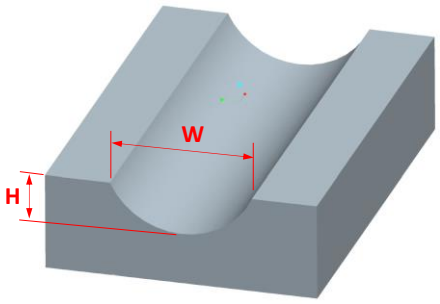

Figure 3. Geometric features of a micro-channel due to AECJM

3. RESULTS AND DISCUSSION

3.1 Modelling with quadratic polynomial

The quadratic polynomial model of channel width (*W*) and channel depth (*H*) are expected to have terms of main factors, two-factor interactions and high order factors. The effect of hierarchy indicates that main factors are more important than two-factor interactions, while two-factor interactions are more important than higher-order factors. For purpose of simplification, this paper eliminated higher-order factors. Thus, the model will be shown as:

$$\boldsymbol{Y = a_0 + \sum_{i=1}^{n} a_i x_i + \sum_{j>i}^{n} a_{ij} x_i x_j} \quad (1)$$

where a_0 is a constant coefficient relating to unchanged process conditions, a_i represents the coefficients of linear terms (main factors), a_{ij} represents the coefficients of two-factor interaction, and n is the total number of main factors. Therefore, the quadratic models of channel width and depth can be described as:

$$\boldsymbol{W = a_0 + a_1 U + a_2 A + a_3 P + a_4 V + a_5 N + a_6 UA + a_7 UP + a_8 UV + a_9 UN + a_{10} AP + a_{11} AV + a_{12} AN + a_{13} PV + a_{14} PN + a_{15} VN} \quad (2)$$

$$\boldsymbol{H = b_0 + b_1 U + b_2 A + b_3 P + b_4 V + b_5 N + b_6 UA + b_7 UP + b_8 UV + b_9 UN + b_{10} AP + b_{11} AV + b_{12} AN + b_{13} PV + b_{14} PN + b_{15} VN} \quad (3)$$

where the *U*, *A*, *P*, *V* and *N* represent working voltage (volt), concentration of abrasive (%), jet pressure (MPa), jet scan speed (mm/s) and number of jet scan passages (integer).

Table 2. Experimental factors and levels.

Level	***U*** (V)	***A*** (wt%)	***P*** (MPa)	***V*** (mm/s)	***N***
1	100	0.3	3	0.04	4
2	130	0.6	3.5	0.06	7
3	160	0.9	4	0.08	10

The necessary data for solving Eqs. (2) and (3) was collected by performance of an orthogonal experiment. Table 2 lists the experimental factors and levels, and Table 3 shows the experimental

design and machining results. The results show that the obtained 27 micro-channels have width varied from 259 to 322 μm, and depth varied from 30 to 181 μm.

Table 3. Experimental design and inspected results**.**

Exp. #	Variable parameters					Achieved results	
	U (V)	***A*** (wt%)	***P*** (MPa)	***V*** (mm/s)	***N***	***W*** (μm)	***H*** (μm)
1	100	0.3	3	0.04	4	259	46
2	100	0.3	3	0.04	7	268	66
3	100	0.3	3	0.04	10	272	90
4	100	0.6	3.5	0.06	4	263	34
5	100	0.6	3.5	0.06	7	282	52
6	100	0.6	3.5	0.06	10	291	76
7	100	0.9	4	0.08	4	296	30
8	100	0.9	4	0.08	7	319	51
9	100	0.9	4	0.08	10	333	64
10	130	0.3	3.5	0.08	4	289	33
11	130	0.3	3.5	0.08	7	303	52
12	130	0.3	3.5	0.08	10	340	69
13	130	0.6	4	0.04	4	308	63
14	130	0.6	4	0.04	7	286	117
15	130	0.6	4	0.04	10	305	150
16	130	0.9	3	0.06	4	277	40
17	130	0.9	3	0.06	7	303	67
18	130	0.9	3	0.06	10	302	100
19	160	0.3	4	0.06	4	307	52
20	160	0.3	4	0.06	7	300	88
21	160	0.3	4	0.06	10	318	129
22	160	0.6	3	0.08	4	293	43
23	160	0.6	3	0.08	7	307	72
24	160	0.6	3	0.08	10	301	102
25	160	0.9	3.5	0.04	4	293	79
26	160	0.9	3.5	0.04	7	301	141
27	160	0.9	3.5	0.04	10	322	181

The coefficients of the models were determined by using the experimental data in Table 3. One main factors and two two-factor interaction, e.g *V*, *AV* and *PV*, have been eliminated from the final equations because the coefficients of a_4, a_{11}, a_{13}, b_4, b_{11} and b_{13} are obtained as zero. Then, the final form of the models are shown as follows:

$$\boldsymbol{W = 480.63 - 2.56U - 176.389A - 58.333P + 1.852N + 1.132UA + 0.635UP + 3.097UV - 0.028UN + 15.556AP + 1.481AN - 0.056PN + 79.167VN} \quad (4)$$

$$\boldsymbol{H = -71.761 + 0.848U - 183.479A + 43.214P - 4.491N + 0.809UA - 0.372UP - 0.806UV + 0.109UN + 19.048AP + 3.611AN + 1.944PN - 144.444VN} \quad (5)$$

3.2 Modelling with dimensional analysis

Besides of working voltage, concentration of abrasive, jet pressure, jet scan speed and jet scan passages, additional five parameters have been introduced into the modelling of channel width and depth in applying dimensional analysis. These five additional processing parameters were selected as jet diameter (*D*), standoff distance (*S*), electrochemical equivalent (ω), density of abrasive (ρ_a) and elastic module of target material (*E*) because the mechanism of material removal is a combination of corrosion and erosion. Thus, the channel width *W* can be expressed as:

$$W = f(U, A, P, V, N, D, \omega, \rho_a, E) \quad (6)$$

Similarly, the channel depth *H* can be described as:

$$H = f(U, A, P, V, N, S, \omega, \rho_a, E) \quad (7)$$

Table 4 lists the dimensions of the ten variables used in modelling of *W* and *H*, where M, L, T, I represent dimensions of mass, length, time and current, respectively.

Table 4. Dimension of variables used in modelling.

Variable	Description	Dimension
U	Working voltage	$ML^2T^{-3}I^{-1}$
A	Concentration of abrasive	1
P	Jet pressure	$MT^{-2}L^{-1}$
V	Jet scan speed	LT^{-1}
N	Number of jet scan passages	1
ω	Electrochemical equivalent	$MI^{-1}T^{-1}$
D	Jet diameter	L
S	Standoff distance	L
ρ$_a$	Density of abrasive	ML^{-3}
E	Elastic module of target material	$MT^{-2}L^{-1}$

According to the Faraday's law, anodic dissolution rate is proportional to potential applied between electrodes (*U*) and is inverse proportional to electrochemical equivalent of metal (ω). Moreover, the mass loss during machining of channel is inverse proportional to jet scan speed (*V*). Thus, the parameters of *U*, ***ω*** and ***V*** can be organized as a dimensionless variable $\frac{U}{\omega V^2}$ which represents the effect of anodic dissolution on machining results of *W* and *H*. Similarly, the parameters of ρ_a, *V* and *P* can be organized as another dimensionless variable $\frac{\rho_a V^2}{P}$ which represents the effect of particles impingement on *W* and *H*. Thus, Eq.(6) and Eq.(7) can be rewritten as following:

$$\frac{W}{D} = k_0 \left[\frac{U}{\omega V^2}\right]^{k_1} \left[\frac{\rho_a V^2}{P}\right]^{k_2} A^{k_3} N^{k_4} \left[\frac{E}{P}\right]^{k_5} \quad (8)$$

$$\frac{H}{S} = q_0 \left[\frac{U}{\omega V^2}\right]^{q_1} \left[\frac{\rho_a V^2}{P}\right]^{q_2} A^{q_3} N^{q_4} \left[\frac{E}{P}\right]^{q_5} \quad (9)$$

where k_0, k_1, k_2, k_3, k_4, k_5, q_0, q_1, q_2, q_3, q_4, q_5 are dimensionless coefficients. The ω is a weighted average equivalent of all composition of stainless steel 316, as listed in Table 5. The values of *D*, *S*, ρ_a and *E* are fixed as 150 μm, 2 mm, 3950 kg/m^3 and 200 GPa in this study.

Table 5. Electrochemical equivalent of each composition of SS316.

Element	Fe	Cr	Ni	Mo	Mn
Composition (%)	66.2	17.0	12.0	2.5	1.5
Equivalent (g/A·h)	1.042	0.6465	1.095	1.193	1.025

The coefficients of k_0, k_1, k_2, k_3, k_4, k_5, q_0, q_1, q_2, q_3, q_4, q_5 in equations (8) and (9) can be solved by using experimental data in Table 3. As a result, the model of channel width and depth turned out to be:

$$W = 1.697 \times 10^4 \left[\frac{U}{\omega V^2}\right]^{0.136} \left[\frac{\rho_a V^2}{P}\right]^{0.179} A^{0.028} N^{0.079} \left[\frac{E}{P}\right]^{-0.429} \quad (\mu m) \quad (10)$$

and

$$H = 2.884 \times 10^{-5} \left[\frac{U}{\omega V^2}\right]^{1.093} \left[\frac{\rho_a V^2}{P}\right]^{0.680} A^{0.107} N^{0.892} \left[\frac{E}{P}\right]^{-1.069} \quad (\mu m) \quad (11)$$

Finally, the equations (10) and (11) can be simplified as:

$$W = 8.2963 \times U^{0.136} V^{0.086} P^{0.250} A^{0.028} N^{0.079} \quad (\mu m) \quad (12)$$

and

$$H = 1.018 \times 10^{-7} U^{1.093} V^{-0.826} P^{0.389} A^{0.107} N^{0.893} \quad (\mu m) \quad (13)$$

3.3 Comparison of validation between two models

Table 6 lists comparison of validation for quadratic polynomial model (model-1) and dimensional analysis model (model-2) using experimental data of Table 3. The prediction of model-1 achieved an average error of 2.1% and a maximum error of 6.6% for channel width, and an average error of 2.7% and a maximum error of 7.8% for channel depth. For the model-2, the averaged and maximum predicted errors of channel width and depth are 2.5% and 8.6%, and 4.3% and 11.1%, respectively. The results show that the prediction of both models agreed well with the experimental data used to solve them. Although the model-1 achieved a little higher accurate prediction than model-2 according to the experiments in Table 3, it doesn't mean that model-1 can perform better than model-2. It seems that the performance of quadratic polynomial model is highly relevant to the experimental variable ranges [23]. The model-1 may not work very well out of the experimental variable ranges. On the other hand, modelling using dimensional analysis can theoretically describe the physical relationship of experimental variables and subsequently show a robust in the performance [18]. This was verified by the additional validation in the following section.

Table 6. Validation of two models with experimental data in Table 3.

Exp.#	Experiments		Prediction of Model-1				Prediction of Model-2			
	W (μm)	*H* (μm)	*W* (μm)	error (%)	*H* (μm)	error (%)	*W* (μm)	error (%)	*H* (μm)	error (%)
1	259	46	258	-0.5	45	-3.3	254	-2.0	41	-11.1
2	268	66	265	-1.0	67	1.9	265	-1.0	67	2.2
3	272	90	273	0.3	90	0.0	273	0.3	93	3.0

4	263	34	274	4.2	35	1.9	279	6.0	33	-1.5
5	282	52	288	2.0	55	5.5	291	3.2	55	6.1
6	291	76	301	3.5	75	-1.2	299	2.9	76	-0.2
7	296	30	295	-0.2	31	1.7	299	0.9	29	-3.2
8	319	51	315	-1.3	48	-5.4	312	-2.2	48	-6.2
9	333	64	334	0.4	66	3.0	321	-3.6	66	2.8
10	289	33	292	0.9	33	-0.7	290	0.5	33	-1.1
11	303	52	306	1.0	51	-2.1	303	0.1	54	3.4
12	340	69	321	-5.7	69	0.0	312	-8.2	74	7.2
13	308	63	289	-6.2	68	7.8	288	-6.4	66	4.2
14	286	117	295	3.2	110	-6.4	301	5.3	108	-7.5
15	305	150	301	-1.2	151	0.8	310	1.6	149	-0.8
16	277	40	277	0.0	38	-4.6	281	1.5	44	9.7
17	303	67	289	-4.5	69	2.3	294	-3.1	72	7.9
18	302	100	302	0.0	99	-1.0	302	0.0	99	-0.6
19	307	52	303	-1.2	50	-3.2	301	-1.9	55	5.2
20	300	88	311	3.5	90	2.1	315	4.9	90	2.5
21	318	129	318	-0.1	129	0.0	324	1.8	124	-3.9
22	293	43	289	-1.3	44	2.9	293	0.0	42	-3.3
23	307	72	303	-1.4	73	0.8	306	-0.3	68	-4.9
24	301	102	316	5.0	101	-1.1	315	4.6	94	-7.7
25	293	79	302	3.2	82	3.9	290	-1.0	82	3.5
26	301	141	308	2.2	134	-5.0	303	0.7	135	-4.5
27	322	181	313	-2.9	186	2.6	312	-3.2	185	2.3

The model-2 shows that the five parameters affect the channel width slightly. This is consistent with the findings of literatures [10,25,26] in which the channel width normally ranged approximate from 150% to 200% of the jet diameter used, although the channel width could be slightly influenced by other parameters. In other words, the jet diameter is the dominant factor affecting channel width. The reason is that the removal of channel depth is higher than that of channel width. Literature [27] demonstrated a two-stage channel formation in jet machining of micro-channel, where a footprint relatively wider than jet diameter is initially formed in the first stage (jet scan passes ≤ 2). After the initial formation of the channels, a second stage of channel formation is hypothesized to occur wherein most of the jet flow from the footprint is directed along the length of the channel rather than radially and up the sidewalls. This would result in decreasing the removal of the sidewalls relative to the channel depth in the region of the footprint. Similar evidence for such behaviour exists in the study of the AWJM [28].

The Eq. 13 shows that channel depth is markedly dependent on working voltage, jet scan speed and jet scan passes. Among these three parameters, the working voltage has the most significance impact on channel depth. This is because the anodic dissolution dominates the material removal in AECJM [26]. In any process of ECM, the mass loss due to anodic dissolution is determined by Faraday's law, wherein the dissolution rate is proportional to the potential drop between electrodes. Higher working voltage would increase higher machining current and therefore result in faster anodic dissolution rate [29,30]. As discussed previously, in the machining of micro-channel, the removal of channel depth is relatively faster than that of sidewall in the second stage of channel formation. As a result, the working voltage obtained the greatest value of power index in Eq. 13.

Predictability is another issue needs to be investigated for the proposed models. A set of experiment with conditions exclusive of Table 3 was conducted to test the two models additionally.

The parameters, selected as extreme conditions in present study, and correspondent machining results are listed in Table 7. Fig. 4 demonstrates the photo and cross-sectional profiles of the machined channels of Table 7. Table 8 lists the validation of quadratic polynomial model and dimensional analysis model according to the experimental data in Table 7.

Table 7. Experiments with extreme conditions.

Exp. code	Variable parameters					Achieved results	
	U (V)	***A*** (wt%)	***P*** (MPa)	***V*** (mm/s)	***N***	***W*** (μm)	***H*** (μm)
Ch-1	100	0.3	3	0.08	4	261	25
Ch-2	100	0.9	3	0.08	4	251	34
Ch-3	160	0.3	4	0.04	10	332	157
Ch-4	160	0.9	4	0.04	10	320	181

The result shows that, for the extreme experiments, the prediction of quadratic model shows a worse agreement than dimensional analysis model. Specifically for experiment coded as "Ch-3", the quadratic model output the channel depth as a negative value which is obviously a fault. This indicates that the quadratic model is only applicable over the parameters' space used for developing the model. On the other hand, the dimensional analysis model agreed with experimental data with an average error of 9% for the four experiments.

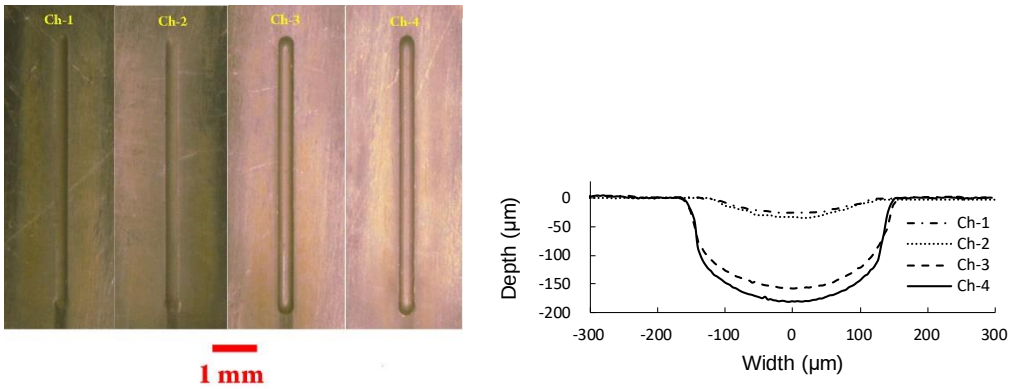

(a) Photos of the channels (b) cross-sectional profiles

Figure 4. Micro-channels machined with extreme conditions.

Table 8. Validation of two models with experiments in Table 7.

Exp.#	Experiments		Prediction of Model-1				Prediction of Model-2			
	W (μm)	*H* (μm)	*W* (μm)	error (%)	*H* (μm)	error (%)	*W* (μm)	error (%)	*H* (μm)	error (%)
Ch-1	261	25	283	8.6	18	-27.3	272	-2.0	23	-11.1
Ch-2	251	34	277	10.3	196	8.2	281	11.8	26	-23.3
Ch-3	332	157	294	-11.4	-0.44	-101.3	316	-4.9	174	10.9
Ch-4	320	181	343	7.3	161	2.5	326	1.7	196	8.2

3.4 Inter-relationship between channel width and channel depth

The presented two models provide a way to control channel width and depth with five processing factors in AECJM machining. However, the width *W* should not be independent of depth *H* because changing any processing parameter will affect *W* and *H* simultaneously. In other words, the *W* interrelates with the *H* for a given machining condition. Thus, it is highly necessary to find out the relationship of channel width and channel depth before applying predictive models.

Figs. 5 and 6 show the main effect of parameters of *U*, *A*, *P*, *V* and *N* on channel width and channel depth respectively, according to the experimental data in Table 3. It can be seen from the Fig. 5 that the machining parameters of *U*=160(V), *A*=0.9(wt%), *P*=4.0(MPa), *V*=0.08(mm/s) and *N*=10 may achieve a maximum width, and the parameters of *U*=100(V), *A*=0.6(wt%), *P*=3.0(MPa), *V*=0.04(mm/s) and *N*=4 will result in a minimum width accordingly. Similarly, the parameters for maximum and minimum depth can be predicted by Fig.6. Table 9 lists geometric features of four channels with maximum *W*, minimum *W*, maximum *H* and minimum *H* predicted by dimensional analysis model. As illustrated in Fig. 7, these four channels contain a region where channel width and channel depth should be reachable concurrently using the predictive model.

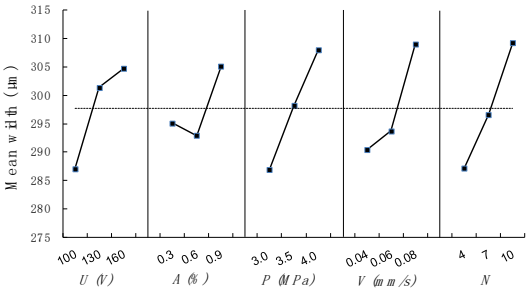

Figure 5. Plot of main effects on channel width.

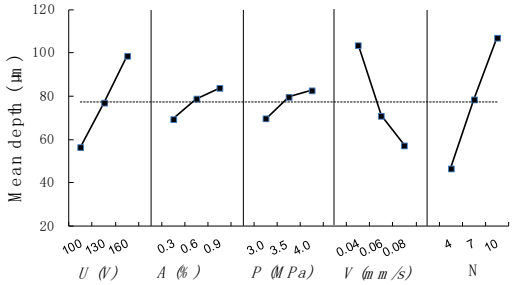

Figure 6. Plot of main effects on channel depth.

Table 9. Prediction of maximum and minimum of width and depth.

Channel code	***U*** (V)	***A*** (wt%)	***P*** (MPa)	***V*** (mm/s)	***N***	Prediction	
						W (μm)	***H*** (μm)
min. ***W***	100	0.6	3	0.04	4	261	44
max. ***W***	160	0.9	4	0.08	10	346	110
min. ***H***	100	0.3	3	0.08	4	272	23
max. ***H***	160	0.9	4	0.04	10	326	196

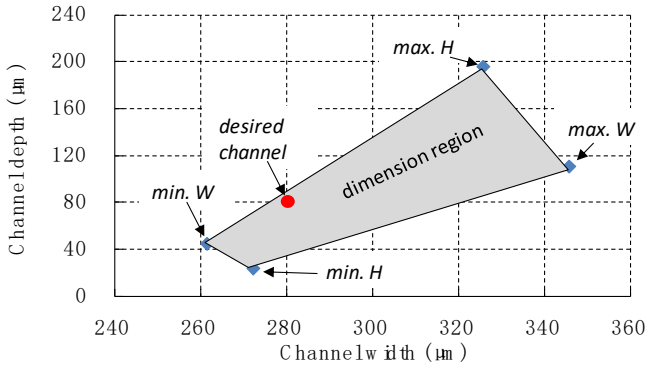

Figure 7. Inter-relationship between channel width and channel depth

3.5 Example of machining with desired width and depth

According to the relationship of the width and the depth in Fig. 7, a target channel with desired *W*=280 μm and *H*=80 μm was selected to verify the present measure to control geometric features in AECJM process. Table 10 lists the process parameters calculated using dimensional analysis model. For consideration of machining efficiency, the *V* and *N* have been assigned as *V*=0.04 mm/s and *N*=4. The jet pressure *P* selected as 3 MPa, and subsequently *A* and *U* were calculated as 0.7 wt% and 170 V which exceeds the space of the working voltage in Table 2. Fig. 8 exhibits six micro-channels machined with parameters in Table 10. Compared with the desired channel width of 280 μm, statistic shows that the 6 channels have a maximum error of 20 μm (7.1%) and an average error of 12.8 μm (4.6%). Similarly, the depths of the 6 channels have a maximum error of 5 μm (6.2%) and an average error of 3.1 μm (3.9%). The result again shows that the prediction of dimensional analysis model agreed well with machining performance. Fig. 9 illustrates two examples of complex micro-channels machined using parameters in Table 10.

Table 10. Desired channel width, depth and calculated parameters.

Desired dimensions		Calculated parameters				
W (μm)	***H*** (μm)	***U*** (V)	***A*** (wt%)	***P*** (MPa)	***V*** (mm/s)	***N***
280	80	170	0.7	3	0.04	4

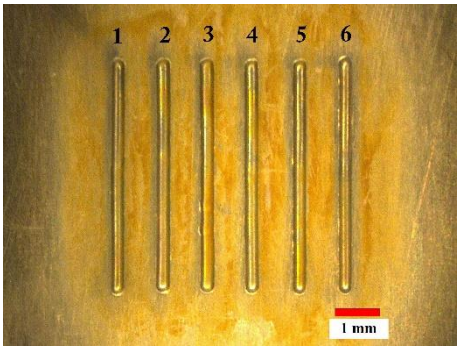

(a) Six machined channels

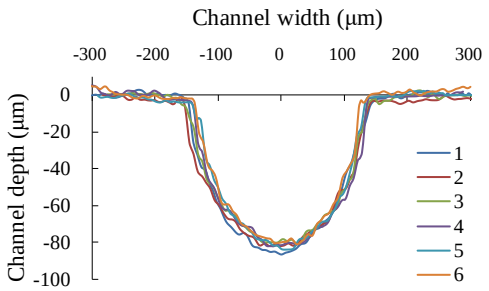

(b) Cross sectional profiles of the six channels

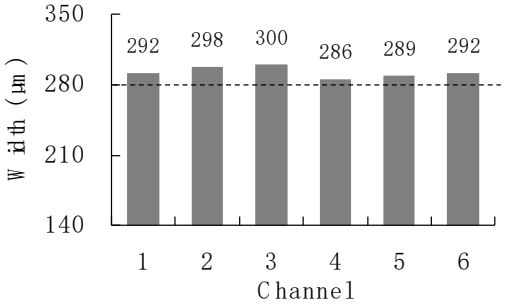

(c) Statistic of channels' width

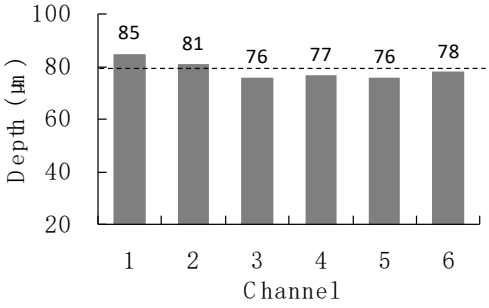

(d) Statistic of channels' depth

Figure 8. Array of micro-channels machined using parameters in Table 10

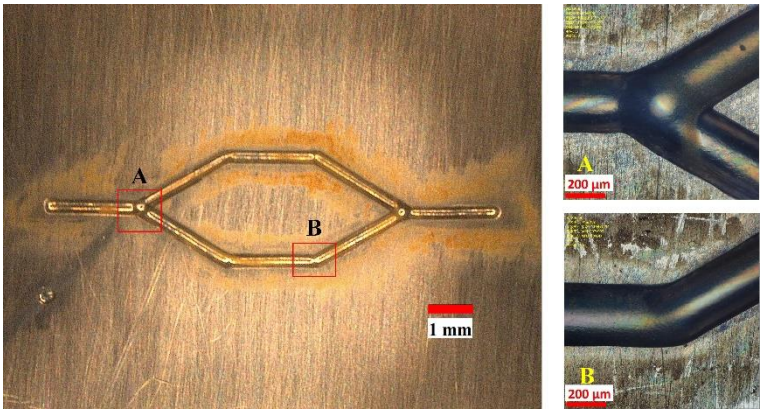

(a)

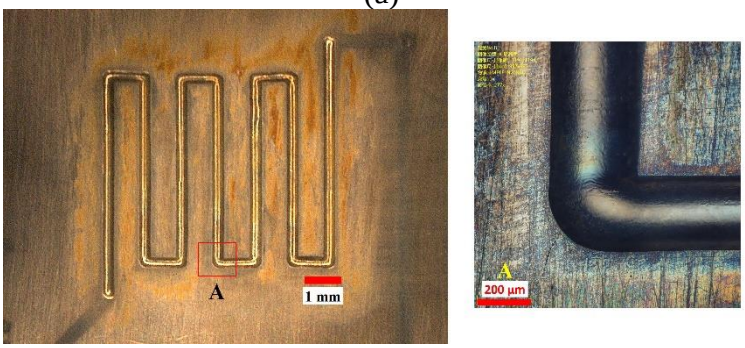

(b)

Figure 9. Machining of complex micro-channels.

4. CONCLUSIONS

This paper presented a method for predicting channel width and channel depth machined using abrasive assisted electrochemical jet machining. Two different models, i.e. quadratic polynomial model and dimensional analysis model, were developed and investigated through experimental data. The following conclusions can be drawn:

(i) Both models have good agreement with experiments within the experimental variables ranges. However, the quadratic polynomial model has the failure possibility to predict result with

parameters outside of the experimental variables ranges. The dimensional analysis model performs more stable than the quadratic polynomial model.

(ii) Jet diameter is the dominant factor affecting the channel width, while other parameters have slight influences on that. This is because most of the jet flow is directed along the length of the channel rather than radially and up the sidewalls after initial formation of machining channel. On the other hand, the channel depth can be significantly affected by working voltage due to the reason that anodic dissolution dominates the material removal in the present process.

(iii) There is an inter-relationship between channel width and channel depth in applying predictive models. This inter-relationship can be graphically expressed through prediction of the maximum and minimum of the width and depth for a given set of process conditions. A target channel can be achieved with desired width and depth according to the relationship and the proposed model.

ACKNOWLEDGEMENTS
The authors acknowledge the support of National Key R&D Program of China (Grant no. 2018YFB1105900) and National Natural Science Foundation of China (Grant no. 51675273).

References

1. CH. Hsu , JC. Jiang, HS. Dang, T. Nguyen, CC Chang, *Microsyst. Technol.*, 24(2018) 255
2. Y. Zhang, S. Wang, P. Ding, *Int. J. Heat. Mass. Tran.*, 113(2017) 295
3. SS. Das, SD. Tilekar, SS. Wangikar, PK. Patowari, *Microsyst. Technol.*, 23(2017) 1
4. A. Walunj, A. Sathyabhama, *Appl. Therm. Eng.*, 128(2018) 672
5. L. Uriarte, A. Herrero, M. Zatarain, G. Santiso, LN. Lopéz de Lacalle, A. Lamikiz, J. Albizuri, *Precis. Eng.*, 31(2007)1
6. SS. Singh, PK. Baruah, A. Khare, SN. Joshi, *Opt. Laser. Technol.*, 99(2018) 107
7. J. Yan, T. Kaneko, K. Uchida, N. Yoshihara, T. Kuriyagawa, *Int. J. Adv. Manuf. Technol.*, 50(2010) 991
8. V. Rathod, B. Doloi, B. Bhattacharyya, *Int. J. Adv. Manuf. Technol.*, 92(2017) 505
9. E. Díaz-Tena, A. Rodríguez-Ezquerro, LN. López de Lacalle Marcaide, LG. Bustinduy, A.E. Sáenz, *J. Clean. Prod.*, 84(2014) 752
10. I. Bisterov, J. Mitchell-Smith, A. Speidel, A. Clare, *Procedia CIRP*, 68(2018) 460
11. N. Haghbin, JK. Spelt, M. Papini, *J. Mater. Process. Tech.*, 222(2018) 399
12. Z. Liu, H. Nouraei, M. Papini, J.K. Spelt, *J. Mater. Process. Technol.*, 214(2014) 1886
13. Y. Zhang, CG. Zhang, H. Dai, Y. Zhu, Y. Ji, *Key. Eng. Mater.*, 579-580(2014) 310
14. ZW. Fan, LW. Hourng, TY. Chen, HP Tsui, *Key. Eng. Mater.*, 749(2017) 148
15. Z. Liu, H. Nouraei, JK. Spelt, M. Papini. *Precis. Eng.*, 40(2015) 189
16. Z. Liu, C. Gao, K. Zhao, C. Guo, *Procedia CIRP*, 68(2018) 719
17. S. Chevalier, C. Josset, B. Auvity, *Renew Energy*, 125(2018) 738
18. V. Ferro, *Catena*, 169(2018) 119
19. J. Kumar, JS. Khamba, *Int. J. Adv. Manuf. Technol.*, 48(2010) 103
20. NG. Patil, PK. Brahmankar, *Int. J. Adv. Manuf. Technol.*, 51(2010) 599
21. B. Jones, ED. Schoen, DC. Montgomery, *Qual. Eng.*, 28(2016) 369
22. M. Sankar, A. Gnanavelbabu, K. Rajkumar, *Procedia Eng.*, 97(2014) 381
23. H. Zhao, S. Li, P. Zou, K Di, *Int. J. Adv. Manuf. Technol.*, 92(2017) 1
24. ST. Kumaran, JK. Tae, M. Uthayakumar, MM. Islam, *J. Alloy Compd.*, 724(2017) 1037
25. A. Martin, M. Hackert-Oschätzchen, N. Lehnert, A Schubert, *Procedia CIRP*, 68(2018) 466

26. Z. Liu, C. Gao, K. Zhao, K. Wang, *Int. J. Adv. Manuf. Technol.*, 95(2018) 1143
27. N. Haghbin, J.K. Spelt, M. Papini, *J. Mater. Process. Technol.*, 222(2015)399
28. N. Haghbin, F. Ahmadzadeh, J.K. Spelt, M. Papini, *Int. J. Adv. Manuf. Technol.*, 84(2016)1031
29. N. Schubert, M. Schneider, A. Michaelis, *Int. J. Refract. Met. Hard Mater*. 47(2014)54
30. M. Hackert-Oschaetzchen, A. Martin, G. Meichsner, M. Zinecker, A. Schubert, *Precis. Eng.*, 37(2013)621.